

Near-ideal relaxed MHD in slab geometry

Arash Tavassoli,¹ Stuart R. Hudson,² Zhisong Qu,³ and Matthew Hole¹

¹*Mathematical Sciences Institute, Australian National University, Acton, ACT 2601, Australia^a*

²*Princeton Plasma Physics Laboratory, PO Box 451, Princeton NJ 08543, USA.^b*

³*School of Physical and Mathematical Sciences, Nanyang Technological University, Singapore 637371, Singapore*

We investigate the solutions of the relaxed MHD model (RxMHD) of Dewar & Qu [J. Plasma Phys. **88**, 835880101 (2022)]. This model is a generalization of Taylor relaxation that allows the ideal Ohm's law constraint to be included, and this offers a pathway to extend the multi-region relaxed MHD (MRxMHD) model. By constructing solutions numerically, we show that the RxMHD model of Dewar & Qu is mathematically well-defined and computationally feasible for constructing MHD equilibria. We also show that a cross-field flow can exist without enforcing an arbitrary constraint on the angular momentum (as is done in the case of MRxMHD with flow), and a pressure profile with a small gradient due to the Bernoulli flow. Our results also demonstrate the self-organization of fully relaxed regions during the optimization, which was an important motivation behind developing this model.

^aElectronic mail: arash.tavassoli@anu.edu.au

^bElectronic mail: shudson@pppl.gov

I. INTRODUCTION

A central challenge in magnetic confinement is constructing a magnetohydrodynamic (MHD) equilibrium that is sufficiently smooth, global, and consistent with the underlying MHD physics. A pioneering equilibrium model was proposed by Kruskal and Kulsrud¹. In this model, the magnetic field is constrained to be tangential to a continuous set of nested flux surfaces, which act as transport barriers and are ergodically covered by magnetic field lines. Therefore, varying the geometry of these surfaces, which from a Hamiltonian mechanical viewpoint are equivalent to the Kolmogorov-Arnold-Moser (KAM) tori², is equivalent to varying the magnetic field. The problem is then reduced to an optimization problem that minimizes a Hamiltonian functional, subject to constraints of ideal MHD. During the optimization, the geometry of magnetic flux surfaces can evolve, while the pressure remains constant on each surface. A well-known problem of this model is that the frozen-in flux constraint of ideal MHD prevents topological changes, magnetic reconnection is excluded and singularities (in the parallel current density) can arise in the solutions. Another issue is that the optimization model is constrained by an infinite set of ideal MHD constraints, and its solutions are highly sensitive to the initial conditions. As a result, these solutions fail to meet a key characteristic of equilibrium: they should be largely independent of the initial conditions, i.e. they should be “global”³. To address these issues, Taylor suggests a heuristic model, known as “Taylor relaxation”, in which from the infinity of constraints of ideal MHD only the conservation of total magnetic helicity is held⁴. The pressure gradient is zero and the magnetic field satisfies the Beltrami equation with a constant multiplier, which can accommodate complicated field lines—phenomena such as islands and chaos. Taylor relaxation has successfully described various phenomena, mainly in the reversed field pinch configuration and spheromaks^{3,5,6}. Nevertheless, Taylor relaxation is too simple to describe the equilibrium in modern fusion devices such as modern tokamaks and stellarators, where a non-constant pressure profile typically peaks at the magnetic axis and decreases towards the plasma edge.

This shortcoming is addressed in Multi-Region Relaxed MHD (MRxMHD). In this model, the nested flux surfaces are discretely positioned in the radial direction and these support all of the pressure gradient. In response, the flux surfaces act as δ -function current sheets which exert an electromagnetic force that balances the exerted pressure gradient. While

the Kruskal–Kulsrud model continuously constrains the geometry, the MRxMHD discretely constrains the geometry. Similar to the Kruskal–Kulsrud model, in MRxMHD, the flux surfaces are assumed to remain resilient against magnetic reconnection while their geometry is optimized to minimize the Hamiltonian functional. In the (sub-)volume enclosed by two consecutive flux surfaces, the pressure is constant and the Taylor relaxation allows the field lines to reconnect and islands to form. The Stepped Pressure Equilibrium Code (SPEC) works based on the same model⁷. Several studies have confirmed the ability of SPEC to construct 3-dimensional (3D) equilibria and even to predict the equilibrium state of tearing instabilities⁸. Newer versions of SPEC can also accommodate the equilibrium with flow^{9,10}, with cross-magnetic field flow added by an angular momentum constraint. However, this constraint (and therefore the resultant cross-field flow) is only applicable in sub-volumes that are bounded by axisymmetric interfaces. This condition is more constraining than requiring axisymmetry only for the outer boundary.

SPEC-like sharp boundary equilibria with prescribed pressure profiles are supported by the KAM theorem and Bruno and Lawrence theorem¹¹ for the systems whose departure from axisymmetry is small. However, neither of these theorems ensures the existence of such equilibria in the presence of arbitrary perturbations. Ref. 12 shows that enforcing indestructible flux surfaces in fixed radial positions along with a stepped pressure profile, as is done in SPEC, might lead to the nonexistence of a solution which manifests as the non-convergence of the numerical algorithm. This happens when the enforced position of flux surfaces coincides with the chaotic field lines of the corresponding single-volume Taylor relaxed state or when the enforced pressure jumps are too large. This problem might be rooted in the fact that in SPEC, the existence of a certain number of relaxed regions is postulated. Another potential problem of MRxMHD is the Taylor relaxation in each volume. Several studies suggest that besides magnetic helicity, other constraints can survive magnetic reconnection^{13–15}. Hence, an extended MRxMHD model that can address these shortcomings seems necessary.

In Ref. 16 the variational formulation of the MRxMHD is developed. This work sets the stage for the extension of Taylor relaxation based on Hamilton’s action principle. Following this principle, Ref. 17 proposes Relaxed MHD (RxMHD) as an extension of single-region Taylor relaxation to a time-dependent problem that includes entropy and cross-helicity constraints as well as the helicity constraint. The basis of RxMHD is the “Ideal MHD Consis-

tency Principle”, meaning solutions of RxMHD are a subset of all possible solutions of the ideal MHD. This principle is guaranteed if the constraints of RxMHD are a subset of the constraints of ideal MHD. Ref. 17 uses a *phase space Lagrangian* instead of a configuration space Lagrangian, which allows for defining two flows; one is the Lagrangian flow which can have both perpendicular and parallel components, and the other one is an exclusively field-aligned flow that sets the cross-helicity constraint. The total flow, defined by the momentum density, is the sum of the two flows and is shown to satisfy the equation of motion of the ideal MHD. Therefore, unlike MRxMHD, the cross-field flow can exist regardless of the axisymmetry attribute of the enclosing boundaries. By introducing a weak form of the ideal Ohm’s law (IOL), Dewar and Qu¹⁸ make this model more consistent with the ideal MHD. Using the augmented Lagrangian method and in several steps, the model is brought closer to the ideal MHD while it does not exactly enforce the IOL. The final model aims to be approximately consistent with ideal MHD, while it is relaxed to an extent just enough to accommodate magnetic reconnection and islands. Therefore, the work of Dewar and Qu¹⁸ can be viewed as a “regularization” of the ideal MHD. This model proposes a pathway for the development of an extended MRxMHD, where the Taylor relaxation in each volume is replaced by RxMHD with a weak IOL constraint. Also, unlike MRxMHD this model allows for the self-organization of relaxed regions during the optimization process, resulting in a more physically reliable approach.

In this work, we demonstrate the first nonlinear numerical solution of the relaxed MHD model proposed by Dewar and Qu¹⁸. Through some numerical tests, we show that the proposed model is well-defined and converges. This work aims to set the stage for developing a numerical code of “extended MRxMHD model”, based on the RxMHD with the IOL constraint.

II. SETUP OF THE EQUILIBRIUM PROBLEM AS A HAMILTONIAN MINIMIZATION PROBLEM

A. The Hamiltonian functional

The Hamiltonian that one needs to minimize is defined in a 3-dimensional (3D) region Ω as

$$H^{MHD}[\mathbf{A}, p, \mathbf{u}, \rho] = \int_{\Omega} \left(\frac{1}{2} \rho u^2 + \frac{1}{2} B^2 + \frac{p}{\gamma - 1} \right) \sqrt{g} \, d^3x, \quad (1)$$

where $\mathbf{A}(\mathbf{x})$ is the magnetic potential vector, $\mathbf{B}(\mathbf{x}) = \nabla \times \mathbf{A}$ is the magnetic field, $p(\mathbf{x})$ is the pressure, γ is the adiabatic index, \sqrt{g} is the Jacobian, and $\mathbf{u}(\mathbf{x})$ is the generalized flow, defined by $\mathbf{u} = \boldsymbol{\pi}/\rho$, where $\boldsymbol{\pi}(\mathbf{x})$ is the momentum density and $\rho(\mathbf{x})$ is the plasma density.

The optimization problem that we define based on the model described in Ref. 18 is

$$\text{Minimize } H^{MHD} \quad \text{Subject to } \Gamma, \quad (2)$$

where Γ is the set of all constraints. The conservation of mass, the kinematic constraint of the Lagrangian flow, and the IOL constraint are ‘‘microscopic’’ constraints; i.e. they are applied pointwise to the whole domain. On the other hand, entropy, helicity, and cross helicity constraints are ‘‘macroscopic’’ constraints; i.e. they are defined extensively as integrals over the Ω . The macroscopic constraints are applied using the Lagrange multiplier method, while the mass conservation and the kinematic constraint are applied explicitly in the variational scheme. The IOL constraint is applied using the augmented Lagrangian method. After adding the relevant constraints, Eq. (1) reads

$$H[\mathbf{A}, p, \phi, \mathbf{u}, \mathbf{v}, \rho, \lambda_s, \lambda_k, \lambda_u] = H^{MHD} + \int_{\Omega} \left(-\lambda_u (\mathbf{u} \cdot \mathbf{B} - U_0) - \lambda_k \left(\frac{1}{2} \mathbf{A} \cdot \mathbf{B} - K_0 \right) - \lambda_s \left(\frac{\rho}{\gamma - 1} \ln \kappa \frac{p}{\rho^\gamma} - S_0 \right) - \boldsymbol{\lambda}_c \cdot \mathbf{C} + \frac{1}{2} \mu C^2 \right) \sqrt{g} \, d^3x, \quad (3)$$

where U_0 , K_0 , and S_0 are the value of the total cross-helicity, helicity, and entropy, respectively, and λ_u , λ_k , and λ_s are their corresponding Lagrange multipliers (which are independent of position). In the definition of entropy, κ is an arbitrary dimensionalizing constant playing the role of density normalisation. The electric potential $\phi(\mathbf{x})$ is defined by $\mathbf{E} = -\nabla \phi$, where $\mathbf{E}(\mathbf{x})$ is the electric field. On the other hand, $\boldsymbol{\lambda}_c(\mathbf{x})$ is a position-dependent vector that enforces the ideal Ohm’s law pointwise,

and \mathbf{C} is defined as

$$\mathbf{C} \equiv \mathbf{E} + \mathbf{v} \times \mathbf{B}. \quad (4)$$

The necessity of the generalized flow \mathbf{u} and its distinction from the other flow \mathbf{v} are explained in Ref. 17. In short, \mathbf{u} is an ingredient of the “phase space Lagrangian” used to avoid inconsistencies arising from applying the cross helicity constraint in the configuration-space-Lagrangian approach, and \mathbf{v} is the kinematically constrained Lagrangian flow velocity. In the Hamiltonian minimization approach, we will see that \mathbf{u} will be a field-aligned velocity while \mathbf{v} will have a cross-field component. Hence, unlike the MRxMHD the cross-field flow can exist in arbitrary geometries.

B. Macroscopic and microscopic constraints

The variation of λ_s , λ_u , and λ_k in Eq. (3) leads to lead to

$$\begin{aligned} \int_{\Omega} \frac{\rho}{\gamma - 1} \ln\left(\kappa \frac{p}{\rho^\gamma}\right) \sqrt{g} d^3x &= S_0, \\ \int_{\Omega} \mathbf{u} \cdot \mathbf{B} \sqrt{g} d^3x &= U_0, \\ \int_{\Omega} \frac{1}{2} \mathbf{A} \cdot \mathbf{B} \sqrt{g} d^3x &= K_0. \end{aligned} \quad (5)$$

During the (hypothetical) variation of the Lagrangian coordinates, density is microscopically constrained by the conservation of mass

$$\delta\rho = -\nabla \cdot \rho\boldsymbol{\zeta}, \quad (6)$$

where $\boldsymbol{\zeta} \equiv \Delta\mathbf{x}$ is the variation Lagrangian coordinates (i.e a “hypothetical” Lagrangian flow). Also, the Lagrangian flow \mathbf{v} is constrained by the kinematic constraint in its static form, i.e.

$$\delta\mathbf{v} = \mathbf{v} \cdot \nabla\boldsymbol{\zeta} - \boldsymbol{\zeta} \cdot \nabla\mathbf{v}. \quad (7)$$

Following Ref. 19 (Chapter 17), we choose $\{\mu^0, \mu^1, \dots\}$ an increasing sequence of numbers that is specified as an input and update $\boldsymbol{\lambda}_c$ as

$$\boldsymbol{\lambda}_c^{N+1} = \boldsymbol{\lambda}_c^N - \mu^N \mathbf{C}^N, \quad (8)$$

so that after each of these iterations (that we call “IOL iterations”), the model comes closer to satisfying the IOL. This means

$$\lim_{N \rightarrow \infty} C^N = 0, \quad (9)$$

i.e. as $N \rightarrow \infty$

$$\mathbf{E} + \mathbf{v} \times \mathbf{B} = 0. \quad (10)$$

However, to avoid the presumptive singularities in the solution¹⁸, the IOL should only be “weakly” satisfied. We note that because of the IOL iterations, all the variable fields as well as λ_c and μ depend on the iteration number N (note that in this work N is not an exponent). For simplifying the notation, however, we keep the N index implicit in our notation unless when it is necessary to show it explicitly.

The recursive relation of Eq. (8) can be solved as

$$\lambda_c^N = \lambda_c^0 - \sum_{N=0}^{\infty} \mu^N \mathbf{C}^N. \quad (11)$$

According to the n-th term test of the divergence of infinite series, the necessary condition for λ_c^∞ to converge is

$$\lim_{N \rightarrow \infty} \mu^N \mathbf{C}^N = 0, \quad (12)$$

which means that for an arbitrarily large N , C should vanish faster than $1/\mu$.

If $\lambda_c = 0$, the last term in (3) serves as a penalty term and the ideal MHD constraint is weakly enforced. Given a fixed μ , the Lagrangian can be extremised to obtain all the physical quantities and Lagrange multipliers, which will, however, depend on the value of μ . To enforce a stronger constraint, one will need to prescribe a very large μ , leading to ill-conditioning. The augmented Lagrangian introduces an additional term λ_c that mitigates the problem of ill-conditioning: one does not need to go to a very high μ to achieve the same level of constraint. Instead, an iterative procedure in Eq. (11) will be used to control the level of constraint. One key objective of this work is to demonstrate the practical feasibility and convergence of the augmented Lagrangian method for enforcing the IOL.

III. EULER LAGRANGE EQUATIONS IN THEIR 3-DIMENSIONAL FORM

The Euler-Lagrange (EL) equations are driven in Ref. 18 in their generic form, from Hamilton’s action principle (by finding the stationary points of the action integral). In our equilibrium problem, the EL equations are obtained from the Hamiltonian minimization and

are slightly different from Ref. 18. The stationary points of Eq. (3) satisfy

$$\rho \mathbf{u} = \lambda_u \mathbf{B}, \quad (13a)$$

$$p = \lambda_s \rho, \quad (13b)$$

$$\nabla \left(\frac{u^2}{2} - \frac{\lambda_s}{\gamma - 1} \ln \kappa \frac{p}{\rho^\gamma} \right) = \mathbf{v} \cdot \nabla \mathbf{w} + \mathbf{w} \cdot \nabla \mathbf{v}, \quad (13c)$$

$$\lambda_k \mathbf{B} + \lambda_u \nabla \times \mathbf{u} - \nabla \times (\mathbf{v} \times (\lambda_c - \mu \mathbf{C})) = \nabla \times \mathbf{B}, \quad (13d)$$

$$\nabla \cdot (\lambda_c - \mu \mathbf{C}) = 0, \quad (13e)$$

where $\mathbf{w} \equiv (\lambda_c - \mu \mathbf{C}) \times \mathbf{B} / \rho$. Eqs. (13a) and (13b) are the results of the variation of \mathbf{u} and p and are the same as Eqs. (B7) and (B9) in Ref. 17, respectively. From Eq. (13b) one can see that λ_s in this model plays the role of the temperature. Eq. (13c) is a result of the variation of the Lagrangian coordinates, which due to Eqs. (6) and (7) results in the variation of both ρ and \mathbf{v} . Eqs. 13 consists of 11 equations, which are to be solved for 12 scalar fields; i.e. $\{p, \rho, \phi\}$ and the components of $\{\mathbf{B}, \mathbf{u}, \mathbf{v}\}$. In the derivation of Eq. (13c), the steady state continuity equation $\nabla \cdot \rho \mathbf{v} = 0$ is used, which is a necessary equation to close the system of Eqs. 13. As we will show later, the simplicity of the geometry chosen in this study allows us to choose \mathbf{v} so that $\nabla \cdot \rho \mathbf{v} = 0$ and two of the equation of Eq. (13c) are trivial. Therefore, three variable fields and three equations are eliminated. We note that $\nabla \cdot \mathbf{B} = 0$ is implied by Eq. (13d).

After some reductions Eqs. 13 read

$$\nabla \left(\lambda_s \ln \frac{\rho}{\rho_\Omega} + \frac{\lambda_u^2 B^2}{2\rho^2} \right) = \mathbf{v} \cdot \nabla \mathbf{w} + \mathbf{w} \cdot \nabla \mathbf{v}, \quad (14a)$$

$$\lambda_k \mathbf{B} - \nabla \times (\mathbf{v} \times (\lambda_c - \mu \mathbf{C})) = \nabla \times \left(1 - \frac{\lambda_u^2}{\rho} \right) \mathbf{B}, \quad (14b)$$

$$\nabla \cdot (\lambda_c - \mu \mathbf{C}) = 0, \quad (14c)$$

where $\rho_\Omega \sim \kappa^{1/\gamma-1}$ is an arbitrary constant. Eq. (14b) is a version of the Beltrami equation modified by the generalized flow \mathbf{u} and the IOL constraint. This equation can be solved along with the modified Bernoulli's equation (Eq. (14a)) and Eq. (14c). Therefore, the system of Eq. (13) is reduced to Eqs. (14a) to (14c), and the variable fields in those equations are reduced to \mathbf{E} , \mathbf{B} , and ρ .

A. Implications of the ideal Ohm's law and comparison with nested flux surfaces

In Kruskal-Kulsrud and multi-region relaxed (MRxMHD) equilibriums, the nested flux surfaces are supported by $\mathbf{B} \cdot \nabla p = 0$ and a monotonic radial pressure profile which is provided as an input. For the static equilibrium with a flow, $\mathbf{B} \cdot \nabla p$ does not necessarily vanish. In our case, Eqs. (13a) and (13b) imply

$$\mathbf{B} \cdot \nabla p = -\frac{\lambda_s}{\lambda_u} \rho^2 \nabla \cdot \mathbf{u}, \quad (15)$$

which is not generally zero. However, if IOL is satisfied in a subdomain $\Theta \subseteq \Omega$ with a finite measure, we have

$$\mathbf{B} \cdot \nabla \phi = 0. \quad (16)$$

From a Hamiltonian mechanical viewpoint, Eq. (16) means that ϕ is a constant of motion, and if it is differentiable and non-constant then magnetic field lines are tangential to a continuous set of nested flux surfaces in Θ . Therefore, one can define a “fully relaxed” state by $\nabla \phi = 0$ in Θ , as also discussed in Refs. 17 and 18. We note that the fully relaxed state differs from the Taylor relaxed state. In this sense, ϕ plays the same role as p in an equilibrium without flow. However, the implications of $\mathbf{B} \cdot \nabla \phi = 0$ and $\mathbf{B} \cdot \nabla p = 0$ differ because in contrast to the pressure profile, the ϕ profile must be a continuous function, otherwise the $E \times B$ drift defined by $\frac{-\nabla \phi \times \mathbf{B}}{B^2}$ (and therefore the kinetic energy) contracts non-physical delta functions.

B. EL equations of a divergence-free \mathbf{v} in the slab geometry

If $\nabla \cdot \mathbf{v} = 0$ then Eqs. (14b) and (14c) read

$$\begin{aligned} \nabla \times \left(1 - \frac{\lambda_u^2}{\rho} \right) \mathbf{B} &= \lambda_k \mathbf{B} + (\mathbf{v} \cdot \nabla)(\boldsymbol{\lambda}_c - \mu \mathbf{E} - \mu \mathbf{v} \times \mathbf{B}) \\ &\quad - (\boldsymbol{\lambda}_c - \mu \mathbf{E} - \mu \mathbf{v} \times \mathbf{B}) \cdot \nabla \mathbf{v}. \end{aligned} \quad (17)$$

Also, if we choose $\boldsymbol{\lambda}_c^0$ ($\boldsymbol{\lambda}_c$ at the initial step of optimization) so that $\nabla \cdot \boldsymbol{\lambda}_c^0 = 0$, then comparing Eqs. (8) and (14c) we have

$$\nabla \cdot \boldsymbol{\lambda}_c^N = 0; \quad N = 0, 1, 2, \dots \quad (18)$$

Therefore, Eq. (14c) reads $\nabla \cdot \mathbf{C} = 0$ or

$$\nabla \cdot \mathbf{E} = -\nabla \cdot (\mathbf{v} \times \mathbf{B}) \quad (19)$$

IV. HAMILTONIAN EXTREMIZATION IN A 1D SLAB GEOMETRY

In a slab geometry, x resembles the radial direction, y resembles the poloidal direction, and z resembles the azimuthal direction of a torus. Our slab has a length 2 that is elongated from $x = -1$ to $x = 1$. We simplify the system of Eq. (13) by assuming that for any scalar f , $\frac{\partial f}{\partial z} = \frac{\partial f}{\partial y} = 0$ (the 1D assumption). Using the gauge freedom, we can assume $\mathbf{A} = \bar{\mathbf{A}} + \nabla g$ so that

$$A_x(x, y, z) = \bar{A}_x(x, y, z) + \frac{\partial g}{\partial x}(x, y, z) = 0, \quad (20a)$$

$$A_y(x, y, z) = \bar{A}_y(x, y, z) + \frac{\partial g}{\partial y}(x, y, z) = \psi_z, \quad (20b)$$

$$A_z(x, 0, z) = \bar{A}_z(x, 0, z) + \frac{\partial g}{\partial z}(x, 0, z) = \psi_y, \quad (20c)$$

where ψ_y and ψ_z are two given constants that play the role of poloidal and toroidal fluxes, respectively. This choice of gauge is also used in SPEC⁷. We note that Eqs. (20b) and (20c) provide some boundary conditions of \mathbf{A} .

The 1D assumption allows us to prescribe \mathbf{v} . In this work, we assume a divergence-free \mathbf{v} given by

$$\mathbf{v} = v^z \hat{z} \equiv \omega x \hat{z}, \quad (21)$$

where ω is a specified constant. The choice of \mathbf{v} is inspired by rigid plasma rotation in an axisymmetric system^{17,20}. We note that Eq. (21) satisfies the continuity equation $\nabla \cdot \rho \mathbf{v} = 0$, so long as $\frac{\partial \rho}{\partial z} = 0$.

A. Two models of the optimization

Regarding the macroscopic constraints, there are two ways in the literature that such optimization problems are solved. One might assume that the Lagrange multipliers λ_s , λ_u , and λ_k are known, solve the Euler-Lagrangian equations, and calculate the S_0 , U_0 , and K_0 in Eq. (5) from the solutions. Conversely, given the S_0 , U_0 , and K_0 , one might find the

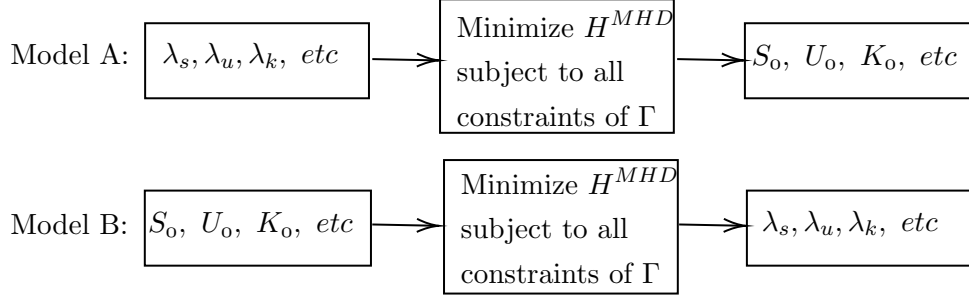


FIG. 1: Two different models of the optimization problem.

Lagrange multipliers by solving Eq. (5) in conjunction with the Euler-Lagrange equations. Fig. 1 shows these two models (named model A and B, respectively) schematically. The technically correct model between these two is model B because only in that model the constraints of Eq. (5) are satisfied. However, model A has some advantages that make it helpful. This model is much simpler to solve because it does not require solving the highly nonlinear equations of Eq. (5), for finding $\lambda_k, \lambda_u, \lambda_s$. This allows us to solve the optimization problem much more easily and even show an approximate analytical solution to the Euler-Lagrange equations, which we use to verify our numerical solution. Also, later when we numerically solve model B, the Lagrange multipliers used in model A provide one of the solutions of model B, provided that we feed the same S_0, U_0 , and K_0 to model B as we have found by solving model A. For this reason, we start solving model A and postpone solving model B to section V.

B. Hamiltonian functional and EL equations in 1D

In the slab geometry, Eq. (1) reads

$$H[\mathbf{A}, p, \phi, \mathbf{u}, \rho] = \int_{-1}^1 \left(\frac{1}{2} \rho u^2 + \frac{1}{2} B^2 + \frac{p}{\gamma - 1} - \lambda_u \mathbf{u} \cdot \mathbf{B} - \lambda_k \frac{1}{2} \mathbf{A} \cdot \mathbf{B} - \lambda_s \frac{\rho}{\gamma - 1} \ln \frac{p}{\rho^\gamma} - \lambda_{cx}(x) C_x(x) + \frac{1}{2} \mu C^2 \right) dx, \quad (22)$$

where $\mathbf{C} = C_x \hat{x} = C \hat{x}$.

Although $\boldsymbol{\lambda}_c$ is generally a vector field, in 1D the $\{y, z\}$ components of \mathbf{C} vanish and $\lambda_{cx}(x) \equiv \lambda_c$ appears as a scalar. Also, Eq. (18) implies that both λ_c and C are independent of position. In 1D, the $\boldsymbol{\nabla} \cdot \mathbf{B} = 0$ implies B_x is constant and this constant should be zero

to satisfy $\mathbf{B} \cdot \hat{n} = 0$ at the boundaries. Therefore

$$\mathbf{B} = B_y \hat{y} + B_z \hat{z} = \partial_x A_y \hat{z} - \partial_x A_z \hat{y}. \quad (23)$$

From this expression of \mathbf{B} and Eq. (21) one can see that, in a 1D slab, the right-hand-side of Eq. (13c) vanishes. In this case, Eqs. (13a), (13b) and (14a) imply

$$p = \lambda_s \rho = \rho_\Omega e^{-u^2/2\lambda_s}. \quad (24)$$

For a small parallel Mach number ($M_\parallel^2 \equiv u^2/\lambda_s \ll 1$), the pressure is approximated as

$$p \approx \lambda_s \rho_\Omega - \lambda_s \rho_\Omega \frac{u^2}{2\lambda_s} + \dots \quad (25)$$

Although we do not use this expansion for constructing a numerical solution, it shows that $\rho = \rho_\Omega$ (corresponding to $p = \lambda_s \rho_\Omega$) is a suitable choice of initial density in our iterative numerical method. Eq. (25) is also used for an approximate analytical solution of the EL equations.

Applying Eqs. (20b) and (20c)

$$\begin{aligned} \int_{-1}^1 B_z dx &= A_y(1) = \psi_z, \\ \int_{-1}^1 B_y dx &= -A_z(1) = \psi_y, \\ A_y(-1) &= A_z(-1) = 0, \end{aligned} \quad (26)$$

which act as boundary conditions of \mathbf{A} . Therefore, in a 1D slab Eqs. (14a), (17) and (19) read

$$\begin{aligned} \lambda_k \mathbf{B} - \omega(\lambda_c - \mu E_x + \mu \omega x B_y) \hat{z} &= \nabla \times \left(1 - \frac{\lambda_u^2}{\rho} \right) \mathbf{B}, \\ \frac{dE_x}{dx} - \omega \frac{dB_y}{dx} &= 0, \\ \lambda_s \ln \frac{\rho}{\rho_\Omega} + \frac{\lambda_u^2 B^2}{2\rho^2} &= 0. \end{aligned} \quad (27)$$

Separating the $\{y, z\}$ components, using $\mathbf{B} = \nabla \times \mathbf{A}$ and $\mathbf{E} = \nabla \phi$,

$$-\lambda_k \frac{dA_z}{dx} = \frac{d}{dx} \left[\left(\frac{\lambda_u^2}{\rho} - 1 \right) \frac{dA_y}{dx} \right] \quad (28a)$$

$$\lambda_k \frac{dA_y}{dx} - \omega \left(\lambda_c + \mu \frac{d\phi}{dx} - \mu \omega x \frac{dA_z}{dx} \right) = \frac{d}{dx} \left[\left(\frac{\lambda_u^2}{\rho} - 1 \right) \frac{dA_z}{dx} \right] \quad (28b)$$

$$\frac{d^2 \phi}{dx^2} = \omega \frac{dx \partial_x A_z}{dx} \quad (28c)$$

$$-\ln \frac{M_\parallel^2}{M_\parallel^2_\Omega} + M_\parallel^2 = 0, \quad (28d)$$

where $M_{\parallel}^2 = \frac{\lambda_u^2 B^2}{\rho^2 \lambda_s} = \frac{u^2}{\lambda_s}$ is the parallel Mach number and $M_{\parallel\Omega}^2 \equiv \frac{\lambda_y^2 B^2}{\rho_{\Omega}^2 \lambda_s}$. Eqs. (28a) and (28b) amount to a modified Beltrami equation. For solving Eq. (28c), we need the potential difference $\Delta\phi = \phi(1) - \phi(-1)$ as an input. A close look at Eq. (28d) shows that if $M_{\parallel\Omega}^2 \leq e^{-1}$, it has two real solutions for M_{\parallel}^2 , otherwise it has no real solution. In the former scenario, one of the solutions is subsonic ($0 < M_{\parallel}^2 \leq 1$) and the other is supersonic $M_{\parallel}^2 \geq 1$. Here, we are only seeking the subsonic solution.

The IOL iterations are proceeded by Eq. (8), which in a 1D slab reads

$$\lambda_c^{N+1} = \lambda_c^N - \mu^N C^N, \quad (29)$$

where $C^N = -\frac{d\phi^N}{dx} + \omega x \frac{dA^{N,z}}{dx}$ and λ_c^N remain independent of x for $N = 0, 1, \dots$. In this work we choose

$$\mu^N = \mu^0 + N\Delta\mu, \quad (30)$$

where $\Delta\mu$ is a specified number. Using this μ , Eq. (11) reads

$$\lambda_c^{\infty} = \lambda_c^0 - \mu^0 \sum_{N=0}^{\infty} C^N - \Delta\mu \sum_{N=0}^{\infty} N C^N. \quad (31)$$

In practice, the infinite series are truncated after $N = N_{max}$.

C. Numerical solution of the nonlinear EL equations

The system of Eq. (28) should be solved within each IOL iteration. To this end, we have used the splitting method, which splits the system of 28 into two operators. Starting with the initial guess $\rho = \rho_{\Omega}$, the Eqs. (28a) to (28c) are solved using the boundary values of Eq. (26) and the finite element method. The solution provides \mathbf{A} and ϕ , which are then used in solving Eq. (28d) for ρ . Wolfram Mathematica²¹ is used for all numerical analysis in this work.

Table I lists the numerical values of the input parameters used for the numerical solution. Among them, ψ_y , ψ_z , λ_k have been tuned so that, if Eqs. (28a) and (28b) are reduced to a Beltrami equation (i.e. $\omega = \lambda_u = 0$), the rotational transform profile reads $\frac{B_y}{B_z} = \tan \lambda_k x$ and $\frac{B_y}{B_z}(x = 1) = \frac{1+\sqrt{5}}{2}$. The λ_u and ω are chosen as relatively small compared to λ_s to resemble the low-Mach-number and high-temperature conditions of stellarator plasmas. In the theoretical formulation of the problem, both κ and ρ_{Ω} are arbitrary parameters; we set

them to 1. The exact choice of the λ_c^0 and the sequence of μ remains essentially arbitrary. After some trial and error, we came up with a sequence of $\mu = 10, 20, 30, \dots, 200$ for updating the λ_c^N values according to Eq. (29).

Fig. 2 shows the numerical solution of different quantities, for the case of $\Delta\phi = 0$. One can see the various stages of the solution's evolution during the IOL iterations, up to $N = 170$, in which the IOL is well satisfied. In this state, the electrostatic potential relaxes to $\phi = 0$; this state corresponds to the fully relaxed state as discussed in Section III A. The rotational transform profile and the component of \mathbf{v} perpendicular to \mathbf{B} ($\mathbf{v}_\perp \equiv \mathbf{v} \cdot \frac{\mathbf{B}}{B}$) also relax to zero. This is expected from Eq. (10) because when $\nabla\phi = 0$, the \mathbf{B} is enforced to align with the prescribed $\mathbf{v} = \omega x \hat{z}$. Fig. 3 shows the solution for a case where $\Delta\phi \neq 0$ ($\Delta\phi = 0.05$). In this case, the solution does not converge to the fully relaxed state, and except at $x = 0$, $\nabla\phi$ remains finite. As a result, a finite \mathbf{v}_\perp appears. Unlike the MRxMHD, this perpendicular flow does not require any restriction on the geometry of boundaries, and therefore, can potentially exist in a 3D equilibrium. In every case, one can see that the pressure rises in the positions where the flow \mathbf{u} drops, as expected for the Bernoulli fluids. According to Eq. (25), the pressure gradient is very small, because in this work we have only considered the pressure (and density) changes resulting from a subsonic flow. This characteristic of p can also be observed in Figs. 2 and 3. To prescribe a monotonic pressure profile similar to modern fusion devices, the model should be expanded to incorporate multiple regions, where pressure jumps between regions are supported by magnetic flux surfaces. This is left for future work.

D. An approximate analytical solution of model A for the small Mach number case

Eq. (28) can be linearized for $M_\parallel^2 \ll 1$ and solved analytically, up to a constant and after the IOL is well satisfied. For $M_\parallel^2 \ll 1$ we approximate ρ with the first term in Eq. (25) ρ_Ω . Using this approximation and assuming that Eq. (12) is satisfied one can show that $N \rightarrow \infty$ Eqs. (28a) and (28b) read

$$-\lambda_k \frac{dA_z}{dx} = \left(\frac{\lambda_u^2}{\rho_\Omega} - 1 \right) \frac{d^2 A_y}{dx^2}, \quad (32a)$$

$$\lambda_k \frac{dA_y}{dx} - \omega \lambda_c^\infty = \left(\frac{\lambda_u^2}{\rho_\Omega} - 1 \right) \frac{d^2 A_z}{dx^2}. \quad (32b)$$

Input parameter	Value(s)	Input parameter	Value(s)
λ_s	8	κ	1
λ_u	0.7	γ	5/3
λ_k	$\arctan\left(\frac{1+\sqrt{5}}{2}\right)$	ω	0.1
ψ_y	0	λ^0	0
ψ_z	1	μ^0	10
$\Delta\phi$	-0.05–0.05	$\Delta\mu$	10
$\rho * \Omega$	1	N_{max}	20

TABLE I: The input parameters used for numerical solutions (for model A).

These equations can be solved analytically and the solution to them gives

$$B_y(x) = \frac{\mathcal{K} \csc(\mathcal{K})}{2\lambda_k^2} [\lambda_k^2 \psi_y \cos(\mathcal{K}x) - \lambda_k(-2\omega\lambda_c^\infty + \lambda_k\psi_z) \sin(\mathcal{K}x)], \quad (33a)$$

$$B_z(x) = \frac{\omega\lambda_c^\infty}{\lambda_k} + \frac{\mathcal{K} \csc(\mathcal{K})}{2\lambda_k^2} [\lambda_k^2 \psi_y \sin(\mathcal{K}x) + \lambda_k(-2\omega\lambda_c^\infty + \lambda_k\psi_z) \cos(\mathcal{K}x)], \quad (33b)$$

where we have introduced a new constant $\mathcal{K} \equiv \frac{\lambda_k}{(\lambda_u^2/\rho\Omega - 1)}$. Although we calculate λ_c^∞ in Eq. (33b) using Eq. (29) and the numerical solutions of C^N , we shall call Eqs. (33a) and (33b) a semi-analytical solution, or for brevity “analytical solution”. Fig. 4 compares the semi-analytical and numerical solutions for different values of λ_u . In this figure, B_y/B_z is the rotational transform and B is the norm of the magnetic field. The parameters used for this figure are again what is listed in Table I. For $\lambda_u \leq 0.5$, one can see an excellent agreement between the analytical and numerical solutions, which validates our numerical results. For $\lambda_u = 0.7$, singularities can be seen in the rotational transition profile close to boundaries where B_z vanishes. Using Eq. (33b), one can calculate that B_z vanishes at about $x \approx \pm 1.017$. In the numerical solution, this point slightly moves to $x \approx \pm 1$.

V. MODEL B OF THE OPTIMIZATION: OPTIMIZATION FOR FIXED ENTROPY, CROSS HELICITY, AND HELICITY

So far in developing the numerical and analytical solutions, we have used model A; i.e we have assumed that λ_s , λ_u , and λ_s are specified. However, in the complete optimization model

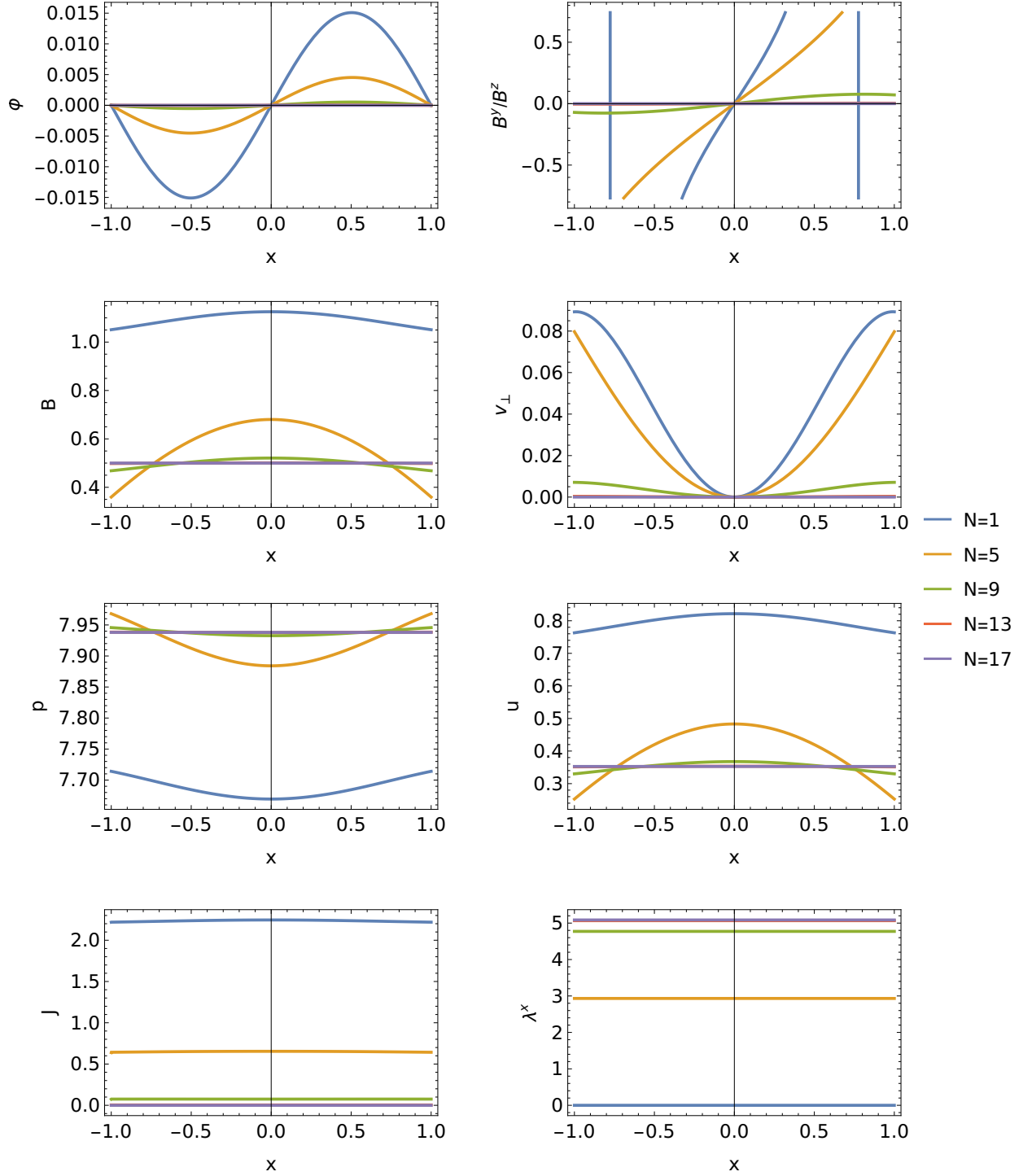


FIG. 2: Solution of Eq. (28) for several values of μ , as the IOL iterations proceed. $\Delta\phi = 0$.

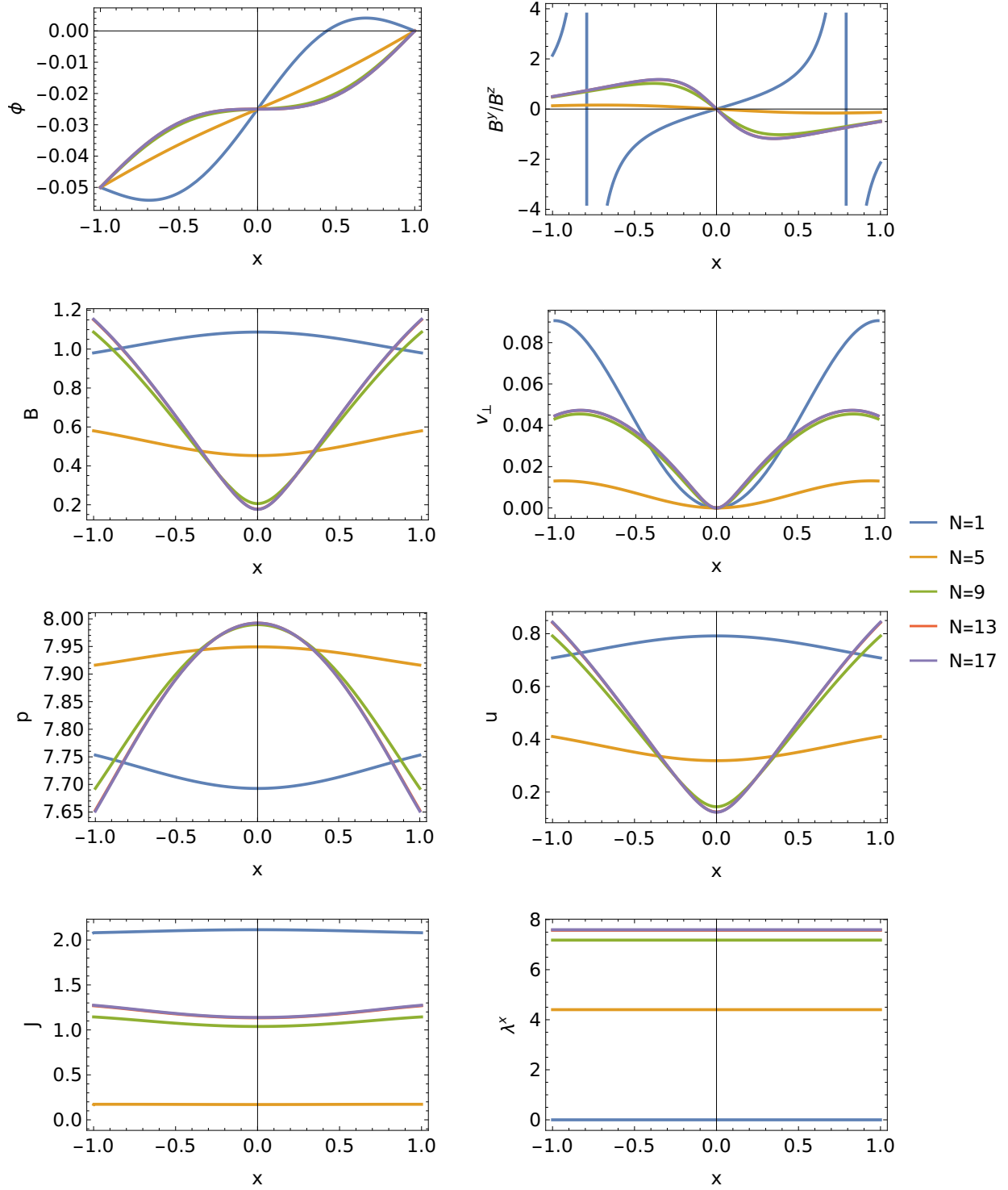


FIG. 3: Solution of Eq. (28) for several values of μ , as the IOL iterations proceed.

$$\Delta\phi = 0.05.$$

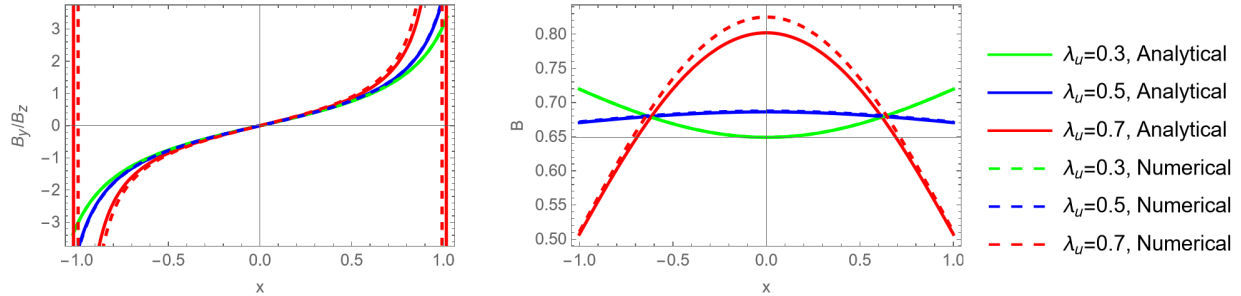


FIG. 4: The comparison of the analytical solution (Eqs. (33a) and (33b)) with the numerical solutions (Eqs. (28a) to (28d)). $\Delta\phi = -0.05$.

(called model B) we should variate these Lagrange multipliers to keep entropy, cross helicity and helicity fixed. To this end, one needs to solve Eqs. 5 along with Eqs. 28. Because Eqs. 5 are highly nonlinear, model B leads to a highly nonlinear problem that is more challenging to solve. Analytical solutions are barely possible in this model, and the computational cost for a numerical solution is significantly increased.

The method we use in the model B of optimization is similar to the shooting method. In this method, the three algebraic equations of 5 are solved for λ_s , λ_u , and λ_k using Newton's method. Because these algebraic equations depend on the variable fields \mathbf{A} , \mathbf{u} , ρ , and \mathbf{p} , within each iteration of Newton's method, we need to solve the system of differential equations of Eq. (28) and provide these variable fields. The initial guess of λ_s , λ_u , and λ_k for the Newton method is always provided by the latest results, except for the first IOL iteration where these values are arbitrarily guessed. Like model A, $\Delta\mu = 10$ is used in model B. An appropriate choice of the value of increment of the penalty parameter $\Delta\mu$ can significantly impact the computational cost of the model. A very large $\Delta\mu$ can lead to difficulties in the convergence of the Newton method, while a very small $\Delta\mu$ necessitates a larger N_{max} which can lead to an increased computational cost.

The report on our numerical results is as follows. In model A, the set of Lagrange multipliers $\{\lambda_s = 8, \lambda_u = 0.7, \lambda_k = 1.01722\}$ is mapped to $\{S_0 = 6.17, U_0 = 0.75, K_0 = -0.18\}$ after 20 IOL iterations. In model B, the same values of $\{S_0, U_0, K_0\}$ are mapped to $\{\lambda_s = 8.00714, \lambda_u = 0.70052, \lambda_k = 1.02735\}$ after 50 IOL iterations. Therefore, the resultant values of Lagrange multipliers in model B are the same as the input values of model A, within an error of less than 1 percent. The convergence of the augmented Lagrangian method in

both models A and B is shown in Fig. 5. In both cases, the convergence is exponential for the large N and the condition $\lim_{N \rightarrow \infty} NC^N = 0$ required for the convergence of series in Eq. (31). However, the convergence of Model A is smoother and faster than that of Model B. Using one processor, the IOL iterations take 1 minute for Model A, while they take about 4 hours for Model B.

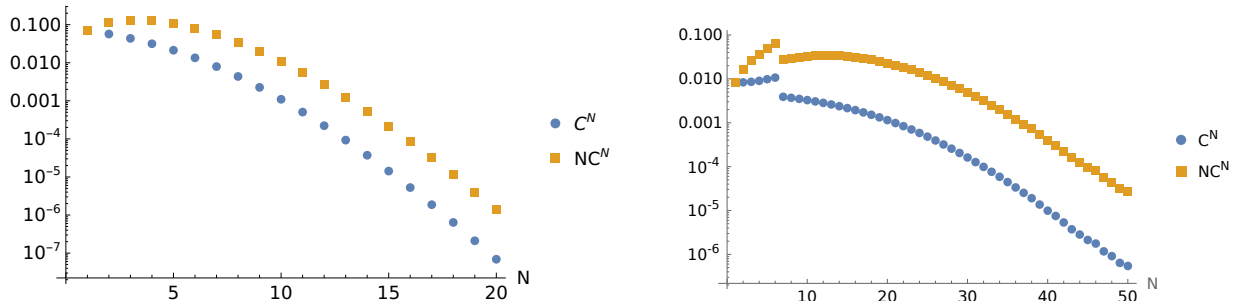


FIG. 5: The convergence of C and NC during IOL iterations. Left) Model A, Right) Model B; $\Delta\phi = 0.05$.

VI. CONCLUSION AND DISCUSSION

The numerical feasibility and convergence of the RxMHD with IOL constraints are demonstrated through a 1-dimensional slab model. The validity of the numerical results is demonstrated by comparing them with analytical solutions. This study is the first step toward an “extended MRxMHD model”.

RxMHD with IOL constraint provides a mathematical framework for the relaxation of the ideal MHD while closely conforming to it. This model can enhance the existing MRxMHD theory by the natural inclusion of the cross-field transport. Although we have not considered the time-dependent case, it has been considered in the original theory. Thus, unlike in MRxMHD, the path to developing a time-dependent code is clear in this model. Unlike SPEC which relies on an input number of relaxed regions, in this model the fully relaxed regions (with $\nabla\phi = 0$) can be self-organized through a mechanism discussed in Section III A and demonstrated numerically in Fig. 2. However, due to assumed geometrical symmetries (the 1D assumption) magnetic islands and chaos cannot be formed in relaxed regions. Applying this model to a 3-dimensional geometry and including multiple sub-regions (separated by pressure jumps) are left for future works.

ACKNOWLEDGMENT

This work was supported by the U.S. Department of Energy under contract number DE-AC02-09CH11466. The United States Government retains a non-exclusive, paid-up, irrevocable, world-wide license to publish or reproduce the published form of this manuscript, or allow others to do so, for United States Government purposes. This work is also supported by Simons Collaboration on Hidden Symmetries and Fusion Energy.

AUTHOR DECLARATIONS

Conflict of interest

The authors have no conflicts to disclose.

DATA AVAILABILITY STATEMENT

The data that support the findings of this study are available from the corresponding author upon reasonable request.

REFERENCES

- ¹M. D. Kruskal and R. Kulsrud, *Equilibrium of a magnetically confined plasma in a toroid* (Princeton University Plasma Physics Laboratory., 1958).
- ²A. J. Lichtenberg and M. A. Lieberman, *Regular and chaotic dynamics*, Vol. 38 (Springer Science & Business Media, 2013).
- ³J. B. Taylor, *Reviews of Modern Physics* **58**, 741 (1986).
- ⁴J. B. Taylor, *Physical Review Letters* **33**, 1139 (1974).
- ⁵H. Bodin, *Nuclear Fusion* **30**, 1717 (1990).
- ⁶M. Yamada, R. Kulsrud, and H. Ji, *Reviews of modern physics* **82**, 603 (2010).
- ⁷S. Hudson, R. Dewar, G. Dennis, M. Hole, M. McGann, G. Von Nessi, and S. Lazerson, *Physics of Plasmas* **19** (2012).
- ⁸J. Loizu, Y.-M. Huang, S. Hudson, D. Bonfiglio, A. Baillo, A. Kumar, and Z. Qu, in *APS Division of Plasma Physics Meeting Abstracts*, Vol. 2021 (2021) pp. PO07–004.

- ⁹Z. Qu, R. L. Dewar, F. Ebrahimi, J. K. Anderson, S. R. Hudson, and M. J. Hole, *Plasma Physics and Controlled Fusion* **62**, 054002 (2020).
- ¹⁰G. Dennis, S. Hudson, R. Dewar, and M. Hole, *Physics of Plasmas* **21** (2014).
- ¹¹O. P. Bruno and P. Laurence, *Communications on pure and applied mathematics* **49**, 717 (1996).
- ¹²Z. S. Qu, S. R. Hudson, R. L. Dewar, J. Loizu, and M. J. Hole, *Plasma Physics and Controlled Fusion* **63**, 125007 (2021).
- ¹³A. Bhattacharjee, R. Dewar, and D. Monticello, *Physical review letters* **45**, 347 (1980).
- ¹⁴A. Yeates, G. Hornig, and A. Wilmot-Smith, *Physical review letters* **105**, 085002 (2010).
- ¹⁵T. Amari and J. Luciani, *Physical Review Letters* **84**, 1196 (2000).
- ¹⁶R. L. Dewar, Z. Yoshida, A. Bhattacharjee, and S. R. Hudson, *Journal of Plasma Physics* **81**, 515810604 (2015).
- ¹⁷R. L. Dewar, J. W. Burby, Z. Qu, N. Sato, and M. Hole, *Physics of Plasmas* **27** (2020).
- ¹⁸R. Dewar and Z. Qu, *Journal of Plasma Physics* **88**, 835880101 (2022).
- ¹⁹J. Nocedal and S. J. Wright, *Numerical optimization* (Springer, 1999).
- ²⁰J. M. Finn and T. Antonsen, *The Physics of fluids* **26**, 3540 (1983).
- ²¹W. R. Inc., *Mathematica*, Version 14.1, champaign, IL, 2024.